A semi-implicit homogeneous discretized differentiator based on two projectors: Experimental validation on a cable-driven parallel robot

Marceau Métillon, Loïc Michel, Stéphane Caro, Malek Ghanes, Franck Plestan, J-P Barbot, Yannick Aoustin

A semi-implicit homogeneous discretized differentiator based on two projectors Experimental validation on a cable-driven parallel robot

L. Michel[a], M. Métillon[a], S. Caro[a], M. Ghanes[a], F. Plestan[a], J. P. Barbot[a,b], Y. Aoustin[a]

a. Nantes Université, École Centrale de Nantes, CNRS, LS2N,
UMR 6004, F-44000 Nantes, France
www.ls2n.fr
b. QUARTZ EA 7393, ENSEA, Cergy-Pontoise, France, France,
https://www.ensea.fr/fr/laboratoire-de-recherche-quartz-51
loic.michel@ec-nantes.fr, marceau.metillon@ls2n.fr, stephane.caro@ls2n.fr,
malek.ghanes@ec-nantes.fr, franck.plestan@ec-nantes.fr, barbot@ensea.fr,
and yannick.aoustin@univ-nantes.fr[1]

Résumé :

Ce travail est dédié à l'application d'un différentiateur semi-implicite et homogène pour estimer la vitesse angulaire et l'accélération angulaire de chacun des huit moteurs électriques du robot parallèle à câbles CRAFT à partir de l'enregistrement de la position angulaire de leur arbre de sortie respectif. Ces moteurs actionnent l'enroulement ou le déroulement de huit câbles pour déplacer la plateforme mobile du robot en translation et en rotation. Les résultats montrent que ce différentiateur, dont la définition est fondée sur deux projecteurs, sont des outils performants pour estimer les vitesses et accélérations angulaires des huit moteurs. Ces vitesses et accélérations estimées sont beaucoup moins bruitées que leurs signaux de référence obtenus par différence arrière. De plus les grandeurs estimées obtenues avec ce différenciateur sont comparées avec succès à celles obtenues par un observateur non-linéaire fondé sur l'interpolation et la différence numérique de la variable de position mesurée. Ces résultats laissent espérer un apport conséquent pour la commande du robot CRAFT.

Abstract :

This work is dedicated to the application of a semi-implicit homogeneous differentiator to estimate the angular velocity and the angular acceleration of each of the eight electric motors of the CRAFT cable-driven parallel robot from the recording of the angular position of their respective output shaft. These motors drive the winding or unwinding of eight cables to move the robot moving-platform. The results show that this differentiator, whose the definition is respectively based on two projectors, is an extremely efficient tool for estimating the angular velocities and accelerations of the eight motors. These estimated velocities and accelerations are much less noisy than their reference signals obtained by backward difference. Moreover, the estimated quantities obtained with this differentiator are successfully compared to those obtained by a non-linear observer based on the interpolation and numerical difference of the measured position variable. Those promising results will definitely contribute to a better control of the CRAFT robot.

[1]Corresponding author

Mots clefs : Robot parallèle à câbles, estimateur de vitesse, estimateur d'accélération, différentiateurs homogènes continus, différentiateurs homogènes discrets, discrétisation semi-implicite d'Euler, projecteurs.

Keywords: cable-driven parallel robot, velocity estimation, acceleration estimation, homogeneous differentiators, homogeneous discretized differentiators, semi-implicit Euler discretization, projectors.

1 Introduction

A cable-driven parallel robot (CDPR) consists of a moving-platform that is connected to a rigid frame by means of cables and actuators, the latter being generally mounted on the ground. Most of the existing robots are powered by electric motors. These robots are very attractive for handling tasks [1–3] because of their low inertia, a higher payload to weight ratio and a large workspace compared to conventional manipulator robots with articulated rigid limbs. A CDPR, named *CRAFT* and located at LS2N, Centrale Nantes campus, is equipped with eight actuators and a moving-platform. Each motor has an encoder sensor measuring the angular velocity of its output shaft allowing to evaluate the performances of the differentiation solutions. The moving-platform has six degrees of freedom. This moving platform is thus over-actuated [4].

The possible application fields of a CDPR can be industrial, or dedicated to search-and-rescue operations. However, for tasks such as motion planning realized with CDPRs, haptic control is still improvable. To deal with various restrictions on cable tensions, cable elasticity, collisions and obstacle avoidance, over-actuation of the moving platform is actually a challenging scientific problem [5], [6].

As a consequence the control of CDPRs is challenging. One key point for their control design is the access, for each electric motor shaft, to the angular variable and its time derivatives. These data are useful to design the robot control in tracking position or in haptic control [7]. Usually, the measurement of the angular variable of the output shaft of each actuator is made thanks to an encoder sensor or a resolver-to-digital converter. However, the measurement of the angular velocity of the output shaft is not usual. Due to weight restrictions, reliability, and financial cost, a tachymeter is not usually available.

A solution to get the value (or the estimation) of the angular velocity can be based on numerical differentiators, which are currently the focus of very active research. For *CRAFT* in order to estimate the angular velocity and angular acceleration from the measured output motor shaft angles the design of continuous time differentiators can be a good solution [8], [9]. However to be closer to physical systems, discretization differentiation is more convenient. The problem of digital differentiation is not new and several methods exist. Diop *et al* [10] investigate interpolation and numerical differentiation for constructing an approach to the design of nonlinear observers. The measured signal is sampled at discrete instants and interpolated by a polynomial for a window data. This elegant method is unfortunately not applicable in real time without introducing delays depending on the computation windows. Real-time discrete signal differentiation has been investigated with sliding-modes techniques. Carjaval-Rubio *et al* [11] derived two discretization algorithms for the homogeneous high-order sliding mode. The main problem to design digital differentiation is how to reject as much as possible the noise effects. Acary & Brogliato [12] introduced an implicit discretization technique, which overcomes some limitations such as the chattering of the classical sliding-mode. They replace the sign function by an implicit projector. Mojallizadeh *et al* [13] develop the implicit discretization scheme for the arbitrary-order super-twisting differentiator. This very effective method has, however, a weakness in some areas, which will be explained in this paper. Semi-implicit discretization is an alternative method that overcomes the implementation difficulties of implicit discretization of homogeneous differentiators. The semi-implicit discretization of various differentiators has been studied and tested. The algorithms for realizing causal systems are provided and semi-implicit schemes are presented to make the implementation straightforward. On the other hand,

for control purpose, Yang *et al* [14] proposed a semi-implicit Euler algorithm for the multivariable super twisting algorithm (STA) in order to attenuate the numerical chattering and preserve its robustness during digital implementations. They analyzed the stability of the semi-implicit Euler implementation algorithm theoretically. Xiong *et al* [15] developed a semi-implicit implementation scheme for the STA with a high control accuracy that is insensitive to the gain overestimation of the STA. A semi-implicit discretization differentiator with one projector was studied in [16] and applied for a nonlinear and non-stationary pneumatic setup [17]. In [18] Yang *et al* presents a digital implementation scheme for the conditioned STA based on a semi-implicit Euler discretization method. Readers can refer to [19] to obtain a good survey with details and a state-of-the-art of differentiation solutions.

Among the numerous algorithms in the framework of the discrete homogeneous differentiation, the proposed differentiator SIHD-2, which combines explicit terms with implicit one including two *projectors* in order to reduce the effects of chattering as well as noise and disturbances, is efficient [20]. This method was chosen to estimate the velocity of the *CRAFT* actuators.

The contribution of this paper is to adapt this algorithm with its parameter in order to estimate both the angular velocity and angular acceleration of each motor shaft of *CRAFT*. Furthermore, the performance of the new numerical differentiation scheme is compared experimentally to the performance of the algorithm proposed by Diop *et al* [10]. This comparison shows that the results of the differentiator are coherent with those of this algorithm for both angular velocity and angular acceleration.

The remaining of the paper is organized as follows. Section 2 is devoted to the presentation of *CRAFT* namely, its geometric, kinematic, and dynamic models. The problem is stated in Sec. 3 in order to present the homogeneous continuous-time differentiator. The semi-implicit Euler discretization is determined in Sec. 4. The experimental results are presented in Sec. 5. Conclusions and future work are drawn in Sec. 6.

2 The cable-driven parallel robot *CRAFT*

This section is dedicated to the description of *CRAFT* and its dynamic model.

2.1 *CRAFT* prototype located at LS2N, Nantes, France.

The cable-driven parallel robot prototype, named *CRAFT* is located at LS2N, France. The base frame of *CRAFT* is 4 m long, 3.5 m wide, and 2.7 m high, see Figure 1. The three-DoF translational motions and the three-DoF rotational motions of its suspended moving-platform (*MP*) are controlled with eight cables being respectively wound around eight actuated reels fixed to the ground. The *MP* is 0.28 m long, 0.28 m wide, and 0.2 m high, its overall mass being equal to 5 kg.

Figure 1: *CRAFT*'s prototype located at LS2N, Nantes, France.

Figure 2 shows the main hardware of the prototype, which consists of a PC (equipped with © MATLAB and © ControlDesk software), eight © PARKER SME60 motors and TPD−M drivers, a © dSPACE DS1007-based real-time controller and eight custom made winches. Each cable can exert a tension up to 150 N to the *MP*. The maximum velocity of each cable is equal to 5.9 m/s. The cable tensions are measured using eight FUTEK FSH04097 sensors, one for each cable, attached to cable anchor points. Their signal is amplified using eight FSH03863 voltage amplifiers and sent to the robot controller by a coaxial cable. Their measurement frequency is 1 kHz.

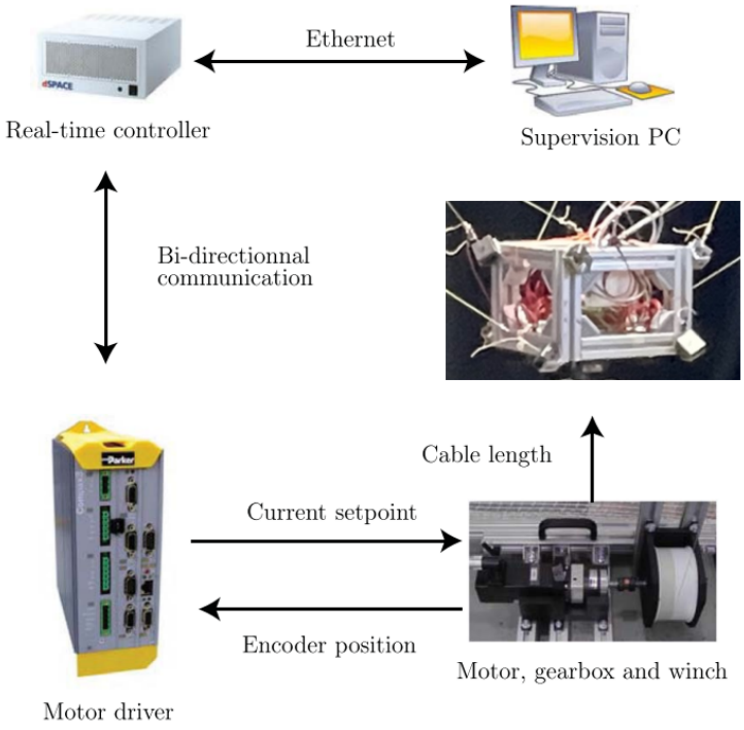

Figure 2: The hardware of the prototype *CRAFT*.

2.2 Dynamic Model

The dynamic model of *CRAFT* used in this paper only considers the mass and inertia of the MP, the latter being pulled by the cables. Indeed, assuming that the diameters of the cables and the pulleys are small, the dynamic effects of the pulleys and the cables are neglected. A more general dynamic model taking into account also the dynamics of the motors, gearboxes, winches could be considered, but would not provide fundamentally different information on the movement of the platform.

As described in [2] the dynamic equilibrium equation of the moving platform is expressed as:

$$\mathbb{I}_p \ddot{\mathbf{p}} + \mathbf{C}\dot{\mathbf{p}} - \mathbf{w}_g = \mathbf{W}\tau + \mathbf{w}_e \tag{1}$$

where $\mathbf{W}$ is the wrench matrix that maps the cable tension vector τ into the wrench exerted by the cables onto the *MP*, and

$$\dot{\mathbf{p}} = \begin{bmatrix} \dot{\mathbf{t}} \\ \omega \end{bmatrix} \quad \ddot{\mathbf{p}} = \begin{bmatrix} \ddot{\mathbf{t}} \\ \alpha \end{bmatrix}, \tag{2}$$

where $\dot{\mathbf{t}} = [\dot{t}_x, \dot{t}_y, \dot{t}_z]^\top$ and $\ddot{\mathbf{t}} = [\ddot{t}_x, \ddot{t}_y, \ddot{t}_z]^\top$ are the vectors of the moving platform linear velocity and acceleration, respectively, while $\omega = [\omega_x, \omega_y, \omega_z]^\top$ and $\alpha = [\alpha_x, \alpha_y, \alpha_z]^\top$ are the vectors of the moving platform angular velocity and acceleration, respectively.

The external wrench $\mathbf{w}_e$ is a 6-dimensional vector expressed in the fixed reference frame $\mathscr{F}_b$ and takes the form

$$\mathbf{w}_e = \left[\mathbf{f}_e^\top, \mathbf{m}_e^\top\right]^\top = [f_x, f_y, f_z, m_x, m_y, m_z]^\top \tag{3}$$

f_x, f_y, and f_z are the x, y, and z components of the external force vector $\mathbf{f}_e$. m_x, m_y, and m_z are the x, y, and z components of the external moment vector $\mathbf{m}_e$, respectively. The components of the external wrench $\mathbf{w}_e$ are assumed to be bounded as follows

$$f_{min} \leq f_x, f_y, f_z \leq f_{max} \tag{4}$$

$$m_{min} \leq m_x, m_y, m_z \leq m_{max} \tag{5}$$

According to (4) and (5), the set $[\mathbf{w}_e]_r$, called the Required External Wrench Set (REWS), that the cables have to balance is a hyper-rectangle.

The *Center of Mass* (*CoM*) of the moving platform, G, may not coincide with the origin of the frame $\mathscr{F}_p$ attached to the platform. The mass of the platform being denoted by M, the wrench $\mathbf{w}_g$ due to the gravity acceleration vector $\mathbf{g}$ is defined as follows

$$\mathbf{w}_g = \begin{bmatrix} M\mathbf{I}_3 \\ \mathbf{M}\hat{\mathbf{S}}_p \end{bmatrix} \mathbf{g} \tag{6}$$

where $\mathbf{I}_3$ is the 3×3 identity matrix, $\mathbf{MS}_p = \mathbf{R}\,[Mx_p, My_p, Mz_p]^\top$ is the first momentum of the moving platform defined with respect to frame $\mathscr{F}_b$. The vector $\mathbf{S}_p = [x_p, y_p, z_p]^\top$ defines the position of G in frame $\mathscr{F}_p$. $\mathbf{M}\hat{\mathbf{S}}_p$ is the skew-symmetric matrix associated with $\mathbf{MS}_p$.

The matrix $\mathbb{I}_p$ represents the spatial inertia of the platform

$$\mathbb{I}_p = \begin{bmatrix} M\mathbf{I}_3 & -\mathbf{M}\hat{\mathbf{S}}_p \\ \mathbf{M}\hat{\mathbf{S}}_p & \mathbf{I}_p \end{bmatrix} \tag{7}$$

where $\mathbf{I}_p$ is the inertia tensor matrix of the moving-platform, which can be computed by the Huygens-Steiner theorem from the moving platform inertia tensor, $\mathbf{I}_g$, defined with respect to the platform *CoM*

$$\mathbf{I}_p = \mathbf{R}\mathbf{I}_g\mathbf{R}^\top - \frac{\mathbf{M}\hat{\mathbf{S}}_p\mathbf{M}\hat{\mathbf{S}}_p}{M} \tag{8}$$

$\mathbf{R}$ is the rotation matrix defining the moving-platform orientation and $\mathbf{C}$ is the matrix of the centrifugal and Coriolis wrenches, defined as

$$\mathbf{C}\dot{\mathbf{p}} = \begin{bmatrix} \hat{\omega}\hat{\omega}\mathbf{M}\mathbf{S}_p \\ \hat{\omega}\mathbf{I}_p\omega \end{bmatrix} \tag{9}$$

where $\hat{\omega}$ is the skew-symmetric matrix associated to ω.

The 3D dynamic model of *CRAFT* is non-linear. In order to perform the most successful positioning or co-manipulation task, the knowledge of the robot state is necessary. *CRAFT* is not equipped with a sensor to measure the velocity of the output motor shaft angles. A numerical derivative of output motor shaft angles is thus required. In the following, a strategy is presented in order to obtain the numerical derivation of the output motor shaft angles.

3 Statement of the problem

The purpose is to estimate the velocity of the angular variable exclusively from the measured position of the output shaft for each of the eight motors. The continuous-time and the Euler implicit state models of

the considered system are presented. Then the homogeneous continuous-time differentiator is introduced and its semi-implicit discretization is finally justified.

3.1 Continuous-time state model systems

The continuous model under consideration is the following one:

$$\Sigma : \left\{ \begin{array}{rcl} \dot{x}_1 & = & x_2 \\ \dot{x}_2 & = & p(t) \\ y & = & x_1 \end{array} \right. \tag{10}$$

where x_1 and x_2 are respectively the angular variable and its velocity; y is the measure signal of x_1, $y \in \mathscr{C}^{\bar{\omega}}$, i.e., y is assumed to be as an analytic signal:

$$y(t+h) = y(t) + \sum_{j=1}^{\infty} y^{(j)}(t) \frac{h^j}{j!} \tag{11}$$

where $y^{(j)}$ denotes the j^{th} time derivative of y and h is the sampling time.
Let $p(t)$ be a bounded perturbation, which is unknown such that there exists:

$$p_M > 0 \ \text{ such that } \ |p(t)| < p_M \ \text{ for all } \ t > 0. \tag{12}$$

Let the following notation be used for the discretized variable:

$$\begin{array}{rcl} \bullet(t = (k+1)h) & = & \bullet^+ \\ \bullet(t = kh) & = & \bullet. \end{array} \tag{13}$$

The perturbation $p(t)$ is assumed to be a constant parameter or a slow variable. This implies that for a sufficient small sampling-time $h > 0$, $p \equiv p^+$. As a consequence an implicit Euler discretization of the continuous-time model can be written with (13) as follows:

$$\left\{ \begin{array}{l} x_1^+ = x_1 + h x_2^+ = x_1 + h(x_2 + h p^+) \\ \\ x_2^+ = x_2 + h p^+ \\ \\ y{=}x_1 \end{array} \right. . \tag{14}$$

3.2 Homogeneous continuous-time differentiator.

Homogeneity approach is very interesting because if for example a local stability is obtained due to the dilatation, this framework allows extending this local property to global settings, [21]. The option of a continuous-time homogeneous differentiator is therefore chosen under the assumption (12) [22], [23].

This differentiator can be written as,

$$\begin{cases} \dot{z}_1 = z_2 + \lambda_1 \mu \lceil \varepsilon_1 \rfloor^{\alpha} \\ \dot{z}_2 = \lambda_2 \mu^2 \lceil \varepsilon_1 \rfloor^{2\alpha - 1} \\ \hat{y} = z_1 \end{cases} \tag{15}$$

where $\alpha \in [0.5\ , 1[$ has to be fixed [24], $\varepsilon_1 = y - z_1$, and the notation $\lceil \bullet \rfloor^{\alpha} = |\bullet|^{\alpha} \mathrm{sgn}(\bullet)$ is adopted along the paper. If $\alpha = 0.5$ the algorithm (15) becomes the super-twisting differentiator [8] that has a very good accuracy with respect to perturbation, but it is more sensitive to noise. If $\alpha = 1$ the algorithm (15) becomes a linear differentiator that has good properties with respect to noise but its accuracy is degraded under perturbation [23]. The degree of homogeneity of the differentiator (15) d is equal to $\alpha - 1$ with respect to dilatation Λ_r with $r = (r_1 = 1, r_2 = 1)$ [22]. Moreover, $\lambda_i > 0$, $i = 1, 2$ are the linear part gains, which are considered and allow to have the eigenvalues of the differentiation error ε_1 in the left part of the complex plane, i.e., the eigenvalues have a negative real part, while the coefficient μ is chosen sufficiently large to cancel the effect of the unknown perturbation $p(t)$.

In order to be closer to the cable-driven parallel robot *CRAFT* and deal with real signal differentiation application, differentiators based on an Euler discretization approach will be designed in the next section.

3.3 Existing Euler discretization of the homogeneous continuous-time differentiator (15)

To design the Euler discretization of the continuous-time homogeneous differentiator (15), several feasible solutions are obtained using explicit, implicit or semi-implicit methods. The semi-implicit method is chosen in this paper for the following reasons.

Among the different Euler discretization methods two can be considered as follows:

- The usual explicit method: z_i and $\dot{z}_i$ for $i = 1,\ 2$ are known at $t_k = kh$ and z_i^+ is calculated such as.

$$z_i^+ = z_i + h\dot{z}_i \tag{16}$$

  With (16) the explicit Euler discretization of the continuous-time differentiator (15) is deduced as follows,

$$\begin{cases} z_1^+ = z_1 + h\left(z_2 + \lambda_1 \mu \lceil \varepsilon_1 \rfloor^{\alpha}\right) \\ z_2^+ = z_2 + h\lambda_2 \mu^2 \lceil \varepsilon_1 \rfloor^{2\alpha - 1}. \end{cases} \tag{17}$$

  This algorithm (17) unfortunately leads to a chattering effect and therefore the numerical solution is not attractive.

- Implicit method: z_i is known, $\dot{z}_i^+$ is chosen such that z_i^+ is equal to.

$$z_i^+ = z_i + h\dot{z}_i^+. \tag{18}$$

With (18) the implicit Euler discretization [12] of the continuous-time differentiator (14) is deduced as follows,

$$\begin{cases} z_1^+ = z_1 + h\left(z_2^+ + \lambda_1 \mu \lceil \varepsilon_1^+ \rfloor^\alpha\right) \\ \\ z_2^+ = z_2 + h\lambda_2 \mu^2 \lceil \varepsilon_1^+ \rfloor^{2\alpha-1}. \end{cases} \tag{19}$$

Subtracting the two equations of (19) from the first two equations of (14) gives:

$$\begin{cases} \varepsilon_1^+ = \varepsilon_1 - h\left(\varepsilon_2^+ + \lambda_1 \mu \lceil \varepsilon_1^+ \rfloor^\alpha\right) \\ \\ \varepsilon_2^+ = \varepsilon_2 + hp^+ - h\lambda_2 \mu^2 \lceil \varepsilon_1^+ \rfloor^{2\alpha-1}. \end{cases} \tag{20}$$

with $\varepsilon_i = x_i - z_i$ $(i = 1,2)$. As it is usually assumed with the implicit Euler method [25], an analyze of the dynamics on the sliding surface $\varepsilon_1^+ = 0$ leads to the following estimation error model:

$$\begin{cases} \varepsilon_1 &= -h\varepsilon_2^+ \\ \\ \varepsilon_2^+ &= \varepsilon_2 + hp^+ \end{cases}. \tag{21}$$

The scalar equations of (21) are similar and the feedback correction terms as function of λ_i $(i = 1,2)$ are removed. There is no possible correction term to reject the influence of the perturbation term p^+ in this error model (21). If the perturbation term p^+ is zero in the second scalar equation of (21), the variable ε_2 is steady stable and equals to a constant. However, the second scalar equation of (21) could have an unstable dynamics when the perturbation term p^+ is non-zero.

A third approach, the semi-implicit homogeneous Euler discretization allows to overcome the drawbacks of these two previous numerical schemes, [16]. The implicit discretization is kept only in the signum multi valued function $\text{sgn}(\varepsilon_1^+)$ while all other terms are explicitly discretized as follows.

$$\begin{cases} z_1^+ = z_1 + h\left(z_2^+ + \lambda_1 \mu |\varepsilon_1|^\alpha \text{sgn}(\varepsilon_1^+)\right) \\ \\ z_2^+ = z_2 + E_1^+ h\lambda_2 \mu^2 |\varepsilon_1|^{2\alpha-1} \text{sgn}(\varepsilon_1^+). \end{cases} \tag{22}$$

That is why this approach is chosen to discretize the continuous-time model (15). This is presented in the next section to design a variant of the semi-implicit homogeneous Euler differentiator, where $\text{sgn}(\varepsilon_1^+)$ is computed to cancel the influence of the past in ε_1^+ dynamic E_1^+ is the convergence flag of ε_1^+.

4 Semi-implicit Homogeneous Euler differentiator based on two projectors (SIHD-2)

The considered semi-implicit Euler discretization differentiator is defined with the acronym SIHD-2 because two projectors $\mathscr{N}_1$ and $\mathscr{N}_2$ are used to design its correction terms [20]. The strategy aims to "generalize" the multi valued sign function $\text{sgn}(\varepsilon_1^+)$ in sliding-based differentiator in order to reduce the chattering and preserve stability properties for high time steps. The two different projectors, $\mathscr{N}_1$ and $\mathscr{N}_2$ are respectively dedicated to the estimation of z_1 and z_2. From the experimental setup *CRAFT* it has been highlighted that the SIHD-2 algorithm offers better performances than with only one projector. As

a result, the semi-implicit homogeneous Euler discretization based on two projectors (SIHD-2) reads as:

$$\begin{cases} z_1^+ = z_1 + h\left(z_2^+ + \lambda_1\mu|\varepsilon_1|^\alpha \mathscr{N}_1\right) \\ \\ z_2^+ = z_2 + E_1^+ h\lambda_2\mu^2|\varepsilon_1|^{2\alpha-1}\mathscr{N}_2. \end{cases} \tag{23}$$

Subtracting the two equations of (23) from the first two of (14) leads to the following estimation error model:

$$\begin{cases} \varepsilon_1^+ = \varepsilon_1 + h\left(\varepsilon_2^+ - \lambda_1\mu|\varepsilon_1|^\alpha \mathscr{N}_1\right) \\ \\ \varepsilon_2^+ = \varepsilon_2 + h\,p^+ - E_1^+ h\lambda_2\mu^2|\varepsilon_1|^{2\alpha-1}\mathscr{N}_2, \end{cases} \tag{24}$$

Here the definition of the projector $\mathscr{N}_1$ and the tuning of the flag E_1^+ are such as:

$$\mathscr{N}_1(\varepsilon_1) := \begin{cases} \varepsilon_1 \in SD \;\; \rightarrow \mathscr{N}_1 = \dfrac{\lceil \varepsilon_1 \rfloor^{1-\alpha}}{\lambda_1\mu h}, \;\; E_1^+ = 1 \\ \\ \varepsilon_1 \notin SD \;\; \rightarrow \mathscr{N}_1 = \text{sign}(\varepsilon_1), \;\; E_1^+ = 0, \end{cases} \tag{25}$$

with the domain of attraction $SD = \{\varepsilon_1 \,/\, |\varepsilon_1| \leq (\lambda_1\mu h)^{\frac{1}{1-\alpha}}\}$.
When $\varepsilon_1 \in SD$ the equality $\varepsilon_1 = h\varepsilon_2$ (remark that this equality is different from the one of (21)) holds, $\mathscr{N}_2$ reads as:

$$\mathscr{N}_2(\varepsilon_1) := \begin{cases} \varepsilon_1 \in SD' \rightarrow \mathscr{N}_2 = \dfrac{\lceil \varepsilon_1 \rfloor^{2(1-\alpha)}}{\lambda_2 h^2\mu^2} \\ \\ \varepsilon_1 \notin SD' \rightarrow \mathscr{N}_2 = \text{sign}(\varepsilon_1), \end{cases} \tag{26}$$

where $SD' = \{\varepsilon_1 \in SD / |\varepsilon_1| \leq (\lambda_1\mu^2h^2)^{\frac{1}{2(1-\alpha)}} \equiv |\varepsilon_2| \leq (\lambda_1\mu^2)^{\frac{1}{2(1-\alpha)}} h^{\frac{\alpha}{1-\alpha}}\}$. The terms $|e_1|^\alpha$ and $|e_1|^{2\alpha-1}$ are the explicit parts while the projectors (the terms $\mathscr{N}_1$ and $\mathscr{N}_2$) refer to the implicit part.

5 Experimental validation

5.1 Condition of data capture

For each of the eight electrical motors an encoder sensor measures the angular variable q_i, $(i = 1, \cdots, 8)$ of its shaft. The eight motors are equipped with a gearbox reducer of ratio $n = 8$. The measured value is divided by n in order to obtain the angular position of the output shaft of the gearbox reducer. The robot *CRAFT* has no tachometer. As a result, there is no reference measurement of angular velocity and hence angular acceleration for each of the eight motors. The reference signals of the rotation velocity and the rotation acceleration are obtained thanks to the algorithm proposed by Diop *et al* [10] and recalled in this section. As this algorithm cannot be used in real time, the comparison with the differentiator SIHD-2 algorithm is made offline. This choice was made because it is well-known robust with respect to measurement noise, which is not the case with conventional methods such as numerical differentiation (see Fig. 6). The sampling period of the acquisition data from the experimental setup is equal to $h = 1$ ms. Of course, it's possible to apply the estimator algorithm proposed by Diop *et al* in real time, i.e., online

by its definition on a moving segmentation window. However, applying this estimator algorithm in real time will cause the estimated angular velocity and acceleration to lag behind the actual angular velocity and acceleration.

5.2 Attenuation noise projectors

The measured angular positions are noisy such as y becomes $y^m = x_1 + \eta$ where η is a measurement noise. The output corrective term ε_1 becomes $\varepsilon_{1m} = y^m - z_1$. As a consequence, a modified projector including a new parameter θ is introduced in order to mitigate the influence of noise. The semi-implicit Euler homogeneous differentiator SIHD 2 becomes:

SIHD-2

$$\begin{cases} z_1^+ = z_1 + h\left(z_2^+ + \lambda_1\mu|\varepsilon_{1m}|^\alpha \mathscr{N}_{\theta_1}\right) \\ \\ z_2^+ = z_2 + E_{\theta_1}^+ h\lambda_2\mu^2|\varepsilon_{1m}|^{2\alpha-1}\mathscr{N}_{\theta_2}, \end{cases} \tag{27}$$

with

$$\mathscr{N}_{\theta_1} := \begin{cases} (1-\theta_1)|\varepsilon_{1m}|^{1-\alpha} < \lambda_1\mu h \quad \rightarrow \mathscr{N}_{\theta_1} = \dfrac{(1-\theta_1)\lceil\varepsilon_{1m}\rfloor^{1-\alpha}}{\lambda_1 h\mu} \\ \\ (1-\theta_1)|\varepsilon_{1m}|^{1-\alpha} \geq \lambda_1\mu h \quad \rightarrow \mathscr{N}_{\theta_1} = \text{sign}(\varepsilon_{1\text{m}}) \end{cases}$$

and

$$\mathscr{N}_{\theta_2} := \begin{cases} (1-\theta_2)\,|\varepsilon_{1m}|^{2(1-\alpha)} < \lambda_2\mu^2h^2 \rightarrow \mathscr{N}_{\theta_2} = \dfrac{(1-\theta_2)\lceil\varepsilon_{1m}\rfloor^{2(1-\alpha)}}{\lambda_2 h^2\mu^2} \\ \\ (1-\theta_2)\,|\varepsilon_{1m}|^{2(1-\alpha)} \geq \lambda_2\mu^2h^2 \rightarrow \mathscr{N}_{\theta_2} = \text{sign}(\varepsilon_{1\text{m}}). \end{cases}$$

5.3 Principle of the observer strategy proposed by Diop *et al*. [10]

For a window of the recorded data $\{y^m_{k-w},\cdots,y^m_k\}$ an interpolating polynomial function of order N is denoted by

$$\hat{y} = a_0 + a_1(t-t_{k-w}) + \cdots + a_N(t-t_{k-w})^N \tag{28}$$

where $t_k = kh$ and w is such that wh defines the length in time of the moving window used for data interpolation and $w+1$ in the number of data points in the window. The coefficients $\{a_0, a_1, \cdots, a_N\}$ are determined from the squares solution of the following over-determined system:

$$\begin{pmatrix} 1 & 0 & \cdots & 0 \\ 1 & h & \cdots & h^N \\ \vdots & \vdots & \vdots & \vdots \\ 1 & wh & \cdots & (wh)^N \end{pmatrix} \begin{pmatrix} a_0 \\ a_1 \\ \vdots \\ a_N \end{pmatrix} = \begin{pmatrix} y_{k-w} \\ y_{k-w+1} \\ \vdots \\ y_k \end{pmatrix} \tag{29}$$

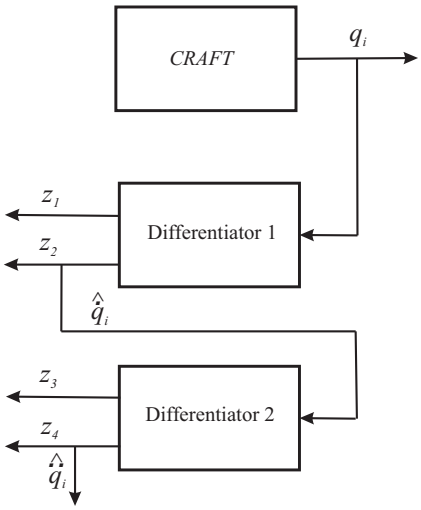

Figure 3: Estimation variables $\hat{\dot{q}}_i$ and $\hat{\ddot{q}}_i$ respectively of the angular velocity and the angular acceleration thanks to the SIHD-2 algorithm with a cascade connection.

with respect to the Euclidean norm. The estimates of the i^{th} time derivatives of y at time t^* are determined by

$$\widehat{\frac{\mathrm{d}^i y_k(t^*)}{\mathrm{d}t^i}} := \left.\frac{\mathrm{d}^i \hat{y}_k(t)}{\mathrm{d}t^i}\right|_{t=t^*} \tag{30}$$

For the experimental tests of this current study the parameters of this numerical differentiation are:

$$W = 2000, \quad N = 4. \tag{31}$$

5.4 Determination of the semi-implicit Homogeneous Euler differentiator parameters

The estimation of the angular velocity $\dot{q}_i$ and the angular acceleration $\ddot{q}_i$ with the SIHD-2 algorithm is carried out by connecting in cascade two SIHD-2 differentiators, which are similar to (27), see Fig. 3. Eight parameters are defined for the SIHD-2 algorithm in : λ_1, λ_2, θ_1 for the differentiator 1, λ_3, λ_4, and θ_2 for the differentiator 2, α, and μ for both. The λ_i, $i = 1,4$ parameters are chosen such that the linear part is stable. The value of homogeneous exponent α is chosen between the coefficient of Levant's differentiator ($\alpha^* = 0.5$) and the linear solution of the discretized differentiator SIHD-2 ($\alpha^* = 1$). The parameters θ_j, $j = 1,2$ is chosen by numerical trial an error allowing a good filtering of the noise, i.e., $0.5 < \theta_j < 1$. The μ parameter is also chosen by numerical test trial and error to determine the best possible action of the projectors $\mathscr{N}_{\theta 1}$ and $\mathscr{N}_{\theta 2}$. The numerical values of these eight parameters are tuned as follows:

$$\begin{aligned} &\lambda_1 = 210, \quad \lambda_2 = 210, \quad \lambda_3 = 525, \quad \lambda_4 = 525, \\ &\alpha = 0.95, \quad \theta_1 = 0.9, \quad \theta_2 = 0.999, \quad \mu = 1. \end{aligned} \tag{32}$$

5.5 Discussion about the experimental results

Figures 4 and 5, present for the eight motors the recorded angular positions of the output shaft, which supports the winch, after the gearbox, and the associate velocities and associate accelerations calculated with the SIHD-2 algorithm. The behavior of the differentiator is quasi uniform whatever the motors. When the platform stops no significant delay can be identified with the velocity and acceleration signals. As there is no tachymeter sensor on the motor shaft, it is difficult to present the backward difference as the one that gives the reference angular velocity and acceleration. Nevertheless, we can evaluate each of the angular velocity signal in terms of their sensitivity to noise. In a common time window, which is equal to 29s-31s and represented by a black dashed line in Fig. 6 the standard deviation is determined for the angular velocity $\hat{\dot{q}}_1$ and the angular acceleration $\hat{\ddot{q}}_1$ respectively estimated with the SIHD-2 method. Remark that the velocity discontinuity at 60 s induces an overshoot with the algorithm, which is proposed by Diop *et*. *al*. It is due to the fact that the polynomial function before 60 s is different from the one after, a constant. With respect to the same phenomenon, SIHD-2 is destabilized at 60 s and converges after a couple of seconds. Table 1 gathers the results for the fourth motor, which represents quite well the general behavior of the eight motors. The sensitivity to noise is much lower for the angular velocity and acceleration signals with the SIHD-2 method than with the backward difference. Figure 6 proves that the results obtained with the differentiator are consistent with those obtained by interpolating the measured positions and the numerical differences of the designed polynomial functions. Although the angular position graph may give the impression of a continuous signal, it is nonetheless a measured signal sampled at the 10 ms period. When digitally derived with the Backward difference method, i.e., the simplest Euler differentiation (function of Matlab *diff*®), we can observe noise, see Fig. 7.

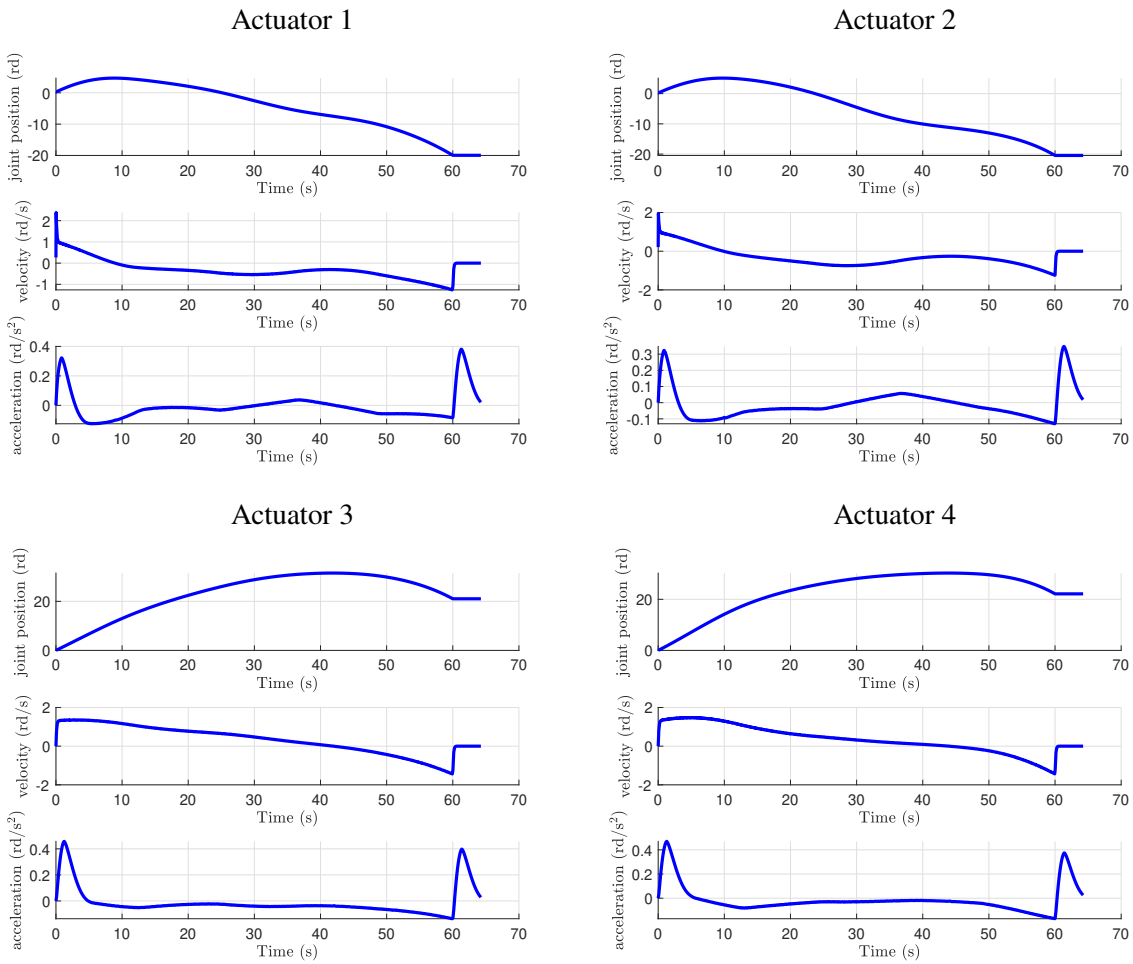

Figure 4: Experimental data for the first four motors: Recording angular positions q_i (radian), estimated angular velocities $\hat{\dot{q}}_i$ (radian s^{-1}), and estimated angular accelerations $\hat{\ddot{q}}_i$ (radian s^{-2}) with the SIHD-2 algorithm, $(i = 1, \cdots, 4)$.

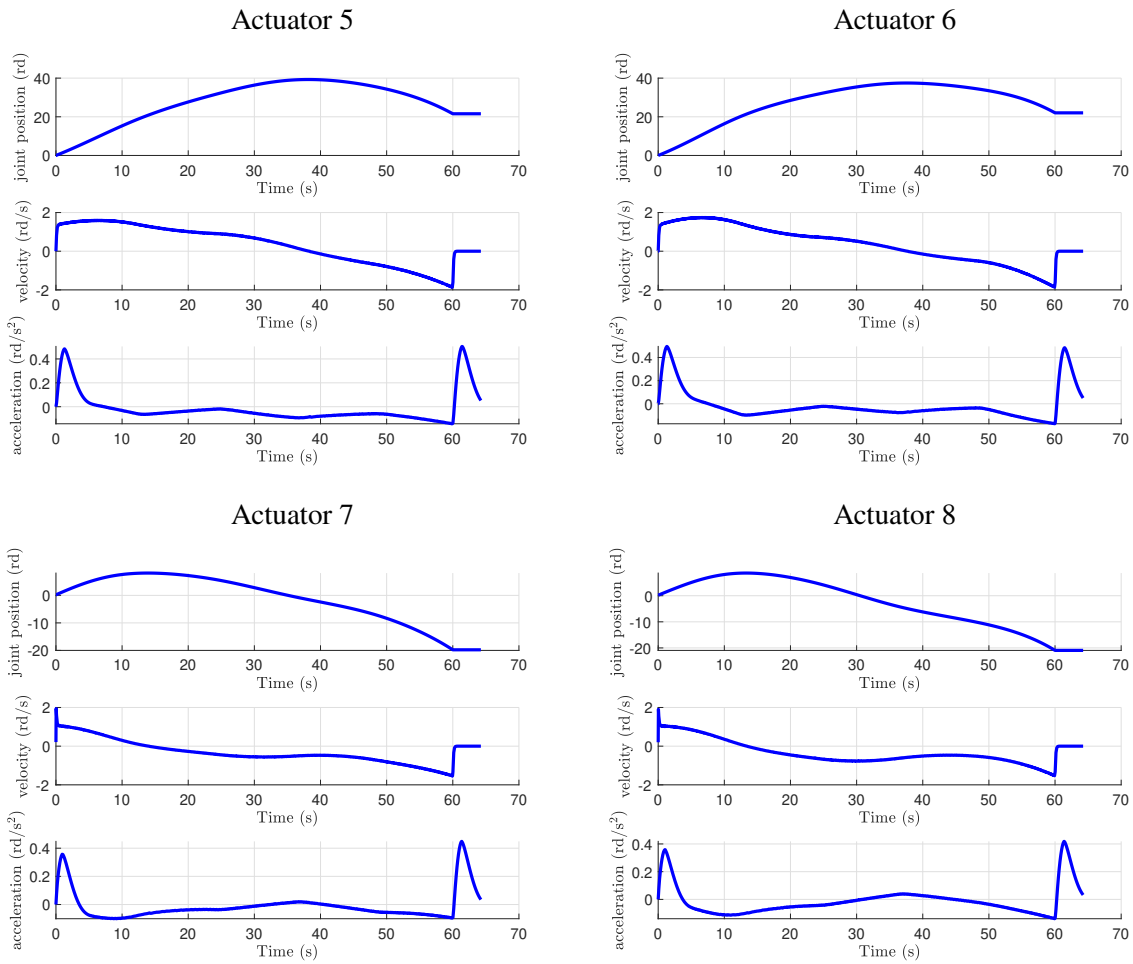

Figure 5: Experimental data for the last four motors: Recording angular positions q_i (radian), estimated angular velocities $\hat{\dot{q}}_i$ (radian s^{-1}), and estimated angular accelerations $\hat{\ddot{q}}_i$ (radian s^{-2}) with the SIHD-2 algorithm, $(i = 5, \cdots, 8)$.

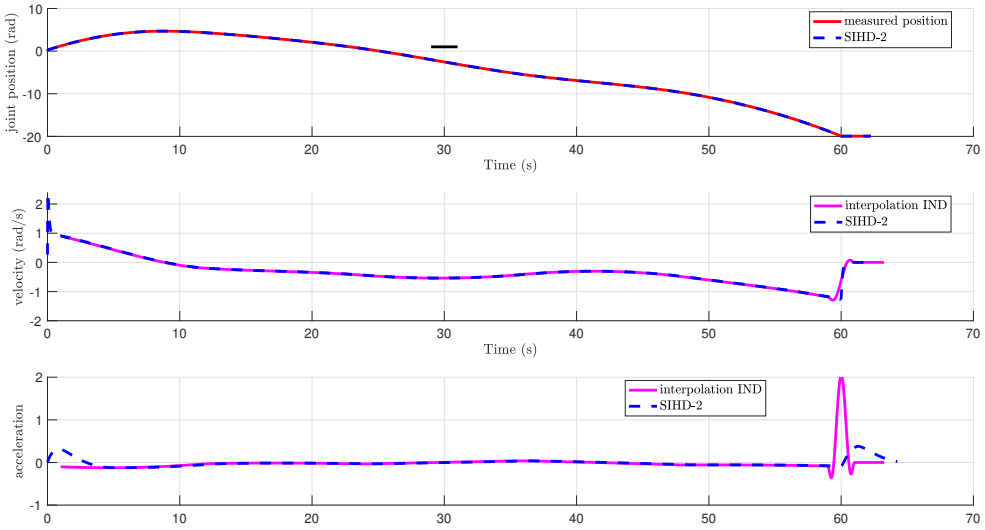

Figure 6: Experimental data for the fourth motor: (top) Recording angular positions defined by (q_1); estimated angular position defined by ($\hat{q}_1$) thanks to the differentiator SIHD-2; (middle) estimated angular velocity $\hat{\dot{q}}_1$ and (bottom) estimated angular acceleration $\hat{\ddot{q}}_1$ respectively thanks to the differentiator SIHD-2 and the observer proposed by Diop *et al*. [10].

Table 1: Standard deviation to evaluate the noise for the angular velocity and the angular acceleration of the fourth motor (BD means Backward difference method).

	angular velocity (rd/s)		angular acceleration (rd/s^2)	
	σ BD	σ SIHD2	σ BD	σ SIHD2
motor 1	0.4021	0.0038	24.7197	0.0036

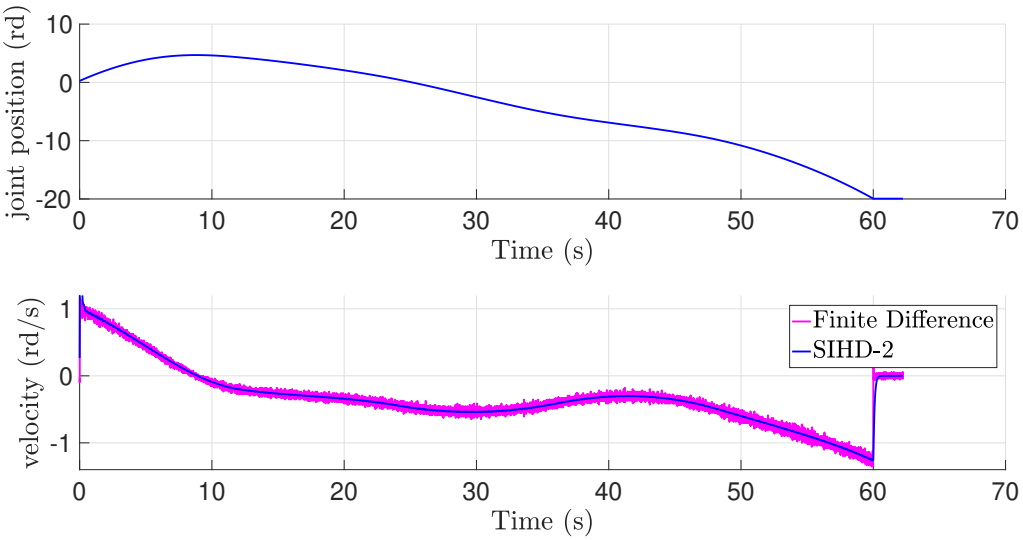

Figure 7: Recording angular positions q_1 (radian), estimated angular velocities $\hat{\dot{q}}_1$ (radian s^{-1}) with the SIHD-2 algorithm, and the Backward difference method.

6 Conclusion

The cable-driven parallel robot *CRAFT* is a complex mechanical system for which the control is difficult due to its over-actuated nature and cable tension constraints. However, its future is promising for applications such as handling, rescue or personal assistance. Two new semi-implicit homogeneous differentiators are applied with success to estimate the angular velocity of the output shaft of the eight motors of the robot *CRAFT*. The obtained velocities are less noisy than those calculated with backward difference.

The results open a great perspective window for this family of robots. First the application of semi-implicit homogeneous differentiators for identification tasks of model parameters such as Coulomb or kinematic frictions, inertia moments, masses could be very efficient. Secondly one important task of a cable-driven parallel robot is the co-manipulation between its effector and human thanks a force sensor. From the measure of a force sensor, a mass parameter allows to deduce an acceleration vector. After a double integration of this acceleration vector a Cartesian trajectory is deduced. Finally, a reference trajectory for each motor can be deduced thanks an inverse geometric model and an inverse kinematic model [7]. The tracking of these reference trajectories has to be perfect with high gain values, from which denoising signals are requested, to obtain an efficient co-manipulation. As a consequence the semi-implicit homogeneous differentiator SIHD-2 will be very useful for the cable-driven parallel robot *CRAFT*.

Acknowledgment

This work was supported by the ANR project DigitSlid ANR-18-CE40-0008-01 (https://anr.fr/Project-ANR-18-CE40-0008) and the ANR CRAFT project, grant ANR-18-CE10-0004 (https://anr.fr/Project-ANR-18-CE10-0004). This work has been partially supported by ROBOTEX 2.0 (Grants ROBOTEX ANR-10-EQPX-44-01 and TIRREX ANR-21-ESRE-0015).

References

[1] E. Picard, S. Caro, F. Plestan, F. Claveau, Control solution for a cable-driven parallel robot with highly variable payload, Vol. Volume 5B: 42nd Mechanisms and Robotics Conference of International Design Engineering Technical Conferences and Computers and Information in Engineering Conference, 2018, p. V05BT07A013. doi:10.1115/DETC2018-85304.

[2] L. Gagliardini, M. Gouttefarde, S. Caro, Determination of a dynamic feasible workspace for cable-driven parallel robots, Proceedings in Advanced Robotics, Springer, 2016, pp. 361–370. doi:doi.org/10.1007/978-3-319-56802-7_38.

[3] H. Tan, L. Nurahmi, B. Pramujati, S. Caro, On the reconfiguration of cable-driven parallel robots with multiple mobile cranes, in: 2020 5th International Conference on Robotics and Automation Engineering (ICRAE), 2020, pp. 126–130. doi:10.1109/ICRAE50850.2020.9310900.

[4] U. A. Mishra, M. Métillon, S. Caro, Kinematic stability based afg-rrt path planning for cable-driven parallel robots, in: 2021 IEEE International Conference on Robotics and Automation (ICRA), 2021, pp. 6963–6969. doi:10.1109/ICRA48506.2021.9560741.

[5] M. Gouttefarde, J.-F. Collard, N. Riehl, C. Baradat, Geometry selection of a redundantly actuated cable-suspended parallel robot, IEEE Transactions on Robotics 31 (2) (2015) 501–510. doi:10.1109/TRO.2015.2400253.

[6] H. Hussein, J. C. Santos, J.-B. Izard, M. Gouttefarde, Smallest maximum cable tension determination for cable-driven parallel robots, IEEE Transactions on Robotics 37 (4) (2021) 1186–1205. doi:10.1109/TRO.2020.3043684.

[7] P. Lemoine, P. P. Robet, M. Gautier, C. Damien, Y. Aoustin, Haptic control of the parallel robot orthoglide, in: 2019 in Proc of the 24td Congrès Français de Mécanique, CFM, Brest, France, 26-30 August, 2019.

[8] A. Levant, Robust exact differentiation via sliding mode technique, Automatica 34 (3) (1998) 379–384. doi:10.1016/S0005-1098(97)00209-4.

[9] A. Levant, Sliding order and sliding accuracy in sliding mode control, International Journal of Control 58 (6) (1993) 1247–1263. doi:10.1080/00207179308923053.

[10] S. Diop, J. Grizzle, P. Moraal, A. Stefanopoulou, Interpolation and numerical differentiation for observer design, in: Proceedings of 1994 American Control Conference - ACC '94, Vol. 2, 1994, pp. 1329–1333 vol.2. doi:10.1109/ACC.1994.752275.

[11] J. E. Carvajal-Rubio, A. G. Loukianov, J. D. Sánchez-Torres, M. Defoort, On the discretization of a class of homogeneous differentiators, in: 2019 16th International Conference on Electrical Engineering, Computing Science and Automatic Control (CCE), 2019, pp. 1–6. doi:10.1109/ICEEE.2019.8884567.

[12] V. Acary, B. Brogliato, Y. V. Orlov, Chattering-free digital sliding-mode control with state observer and disturbance rejection, IEEE Transactions on Automatic Control 57 (5) (2012) 1087–1101. doi:10.1109/TAC.2011.2174676.

[13] M. M. Rasool, B. Brogliato, V. Acary, Time-discretizations of differentiators: Design of implicit algorithms and comparative analysis, Int. J. of Robust and Nonlinear Control 31 (16) (2021). doi:10.1002/rnc.5710.

[14] X. Yang, X. Xiong, Z. Zou, Y. Lou, S. Kamal, J. Li, Discrete-time multivariable super-twisting algorithm with semi-implicit Euler method, IEEE Transactions on Circuits and Systems II: Express Briefs 69 (11) (2022) 4443–4447. doi:10.1109/TCSII.2022.3182772.

[15] X. Xiong, G. Chen, Y. Lou, R. Huang, S. Kamal, Discrete-time implementation of super-twisting control with semi-implicit Euler method, IEEE Transactions on Circuits and Systems II: Express Briefs 69 (1) (2022) 99–103. doi:10.1109/TCSII.2021.3078526.

[16] L. Michel, M. Ghanes, F. Plestan, Y. Aoustin, J.-P. Barbot, Semi-implicit Euler discretization for homogeneous observer-based control: one dimensional case, IFAC-PapersOnLine 53 (2) (2020) 5135–5140, 21st IFAC World Congress. doi:https://doi.org/10.1016/j.ifacol.2020.12.1152.

[17] L. Michel, S. Selvarajan, M. Ghanes, F. Plestan, Y. Aoustin, J. P. Barbot, An experimental investigation of discretized homogeneous differentiators: pneumatic actuator case, IEEE Journal of Emerging and Selected Topics in Industrial Electronics 2 (3) (2021) 227–236. doi:10.1109/JESTIE.2021.3061924.

[18] X. Yang, X. Xiong, Z. Zou, Y. Lou, Semi-implicit Euler digital implementation of conditioned super-twisting algorithm with actuation saturation, IEEE Transactions on Industrial Electronics 70 (8) (2023) 8388–8397. doi:10.1109/TIE.2022.3229380.

[19] M. R. Mojallizadeh, B. Brogliato, A. Polyakov, S. Selvarajan, L. Michel, F. Plestan, M. Ghanes, J.-P. Barbot, Y. Aoustin, A survey on the discrete-time differentiators in closed-loop control systems: Experiments on an electro-pneumatic system, Control Engineering Practice 136 (2023) 105546. doi:10.1016/j.conengprac.2023.105546.

[20] L. Michel, M. Ghanes, F. Plestan, Y. Aoustin, J.-P. Barbot, Semi-implicit homogeneous Euler differentiator for a second-order system: Validation on real data, in: 2021 60th IEEE Conference on Decision and Control (CDC), 2021, pp. 5911–5917. doi:10.1109/CDC45484.2021.9682797.

[21] L. Rosier, Homogeneous Lyapunov function for homogeneous continuous vector field, Systems Control Letters 19 (6) (1992) 467–473. doi:https://doi.org/10.1016/0167-6911(92)90078-7.

[22] W. Perruquetti, T. Floquet, E. Moulay, Finite-time observers: Application to secure communication, IEEE Transactions on Automatic Control 53 (1) (2008) 356–360. doi:10.1109/TAC.2007.914264.

[23] M. Ghanes, J.-P. Barbot, L. Fridman, A. Levant, R. Boisliveau, A new varying-gain-exponent-based differentiator/observer: An efficient balance between linear and sliding-mode algorithms, IEEE Transactions on Automatic Control 65 (12) (2020) 5407–5414. doi:10.1109/TAC.2020.2973609.

[24] Y. Hong, J. Huang, Y. Xu, On an output feedback finite-time stabilization problem, IEEE Transactions on Automatic Control 46 (2) (2001) 305–309. doi:10.1109/9.905699.

[25] V. Acary, B. Brogliato, Implicit euler numerical scheme and chattering-free implementation of sliding mode systems, Systems Control Letters 59 (5) (2010) 284–293. doi:https://doi.org/10.1016/j.sysconle.2010.03.002.